CONFIDENTIAL

Copy 5
RM L57G11

NACA RM L57G11

RESEARCH MEMORANDUM

FREE-FLIGHT INVESTIGATION OF JET EFFECT ON THE LOW-LIFT DRAG AND LONGITUDINAL TRIM OF A SUPERSONIC INTERCEPTOR-TYPE AIRPLANE CONFIGURATION WITH AN OVERHANGING TAIL BOOM AT MACH NUMBERS FROM 1.09 TO 1.34

By Willard S. Blanchard, Jr.

Langley Aeronautical Laboratory
Langley Field, Va.

CLASSIFIED DOCUMENT

NATIONAL ADVISORY COMMITTEE
FOR AERONAUTICS

WASHINGTON

September 19, 1957

CONFIDENTIAL

NATIONAL ADVISORY COMMITTEE FOR AERONAUTICS

RESEARCH MEMORANDUM

FREE-FLIGHT INVESTIGATION OF JET EFFECT ON THE LOW-LIFT DRAG AND LONGITUDINAL TRIM OF A SUPERSONIC INTERCEPTOR-TYPE AIRPLANE CONFIGURATION WITH AN OVERHANGING TAIL BOOM AT MACH NUMBERS FROM 1.09 TO 1.34

By Willard S. Blanchard, Jr.

SUMMARY

A rocket-powered free-flight model of an interceptor-type airplane with an overhanging tail boom was flight tested with jet on and jet off at Mach numbers from 1.09 to 1.34. The jet nozzle, which had a sonic exit, was canted 5° downward with respect to the airplane reference line. Reynolds number, based on wing mean aerodynamic chord, varied from 5.0×10^6 to 10.2×10^6, respectively. Jet static-pressure ratio varied from 2.85 at a Mach number of 1.09 to 3.3 at a Mach number of 1.34. External-drag coefficient was reduced by an amount that varied from 0.006 at a Mach number of 1.09 to zero at a Mach number of 1.26. At Mach numbers greater than 1.26, the effect of jet operation on external drag was adverse. Jet operation induced an upload on the tail and reduced the total drag in the transonic range. The model trimmed approximately 0.25° nose down with power off, and jet operation increased this angle to about -1.0°. The airplane lift-curve slope was not appreciably affected by the jet.

INTRODUCTION

A great deal of attention has been focused on the effects of jet exhaust on the drag, trim, and stability of aircraft. Recent investigations (refs. 1 to 5) have indicated that these effects can be sufficiently large to alter the aerodynamic characteristics of an airplane configuration.

The Langley Pilotless Aircraft Research Division has conducted a rocket-powered free-flight test of an interceptor-type model with an overhanging tail boom to ascertain the effect of jet exhaust on low-lift drag and longitudinal trim. The configuration tested was conventional in general geometry, and consisted of a swept and tapered wing

of 4-percent thickness mounted on a slim (fineness ratio 14.2) fuselage. The horizontal and vertical tails, which were geometrically similar to the wing, were mounted on a boom above and behind the jet exit. The fuselage did not include an inlet since, in the test technique used, the hot turbojet exhaust was simulated by the flow from a rocket motor.

In order to maintain a measure of practicality for the test reported herein, the model was designed to include, volume-wise, equipment required for a present-day (M = 1.6) interceptor airplane. Based on a hypothetical airplane having 384 square feet of wing area, the model was 1/10 scale.

SYMBOLS

M	free-stream Mach number
R	Reynolds number based on mean aerodynamic chord
V	velocity, ft/sec
q	dynamic pressure, lb/sq ft
W	model weight, lb
$\bar{c}$	mean aerodynamic chord
S	wing area (leading and trailing edges extended to fuselage center line), 3.84 sq ft
α	angle of attack, deg
α_o	angle of attack at zero lift, deg
C_a	axial-force coefficient, $\frac{\text{Axial force}}{qS}$
C_D	external-drag coefficient, $\frac{\text{External drag}}{qS}$
C_N	normal-force coefficient, $\frac{\text{Normal force}}{qS}$
C_L	lift coefficient, $\frac{\text{Lift}}{qS}$

C_T thrust coefficient, $\frac{\text{Thrust}}{qS}$

C_{L_o} lift coefficient at zero angle of attack

C_{L_α} lift-curve slope, $\frac{\partial C_L}{\partial \alpha}$, per deg

t time, sec

A cross-sectional area

l model length, in.

x distance measured rearward from nose, in.

a_l/g longitudinal accelerometer reading

a_n/g normal accelerometer reading

p_∞ free-stream static pressure, lb/sq in.

g acceleration due to gravity, 32.2 ft/sec^2

Δ increment resulting from jet operation

γ flight-path angle, deg

p_j jet-exit static pressure, lb/sq in.

A_j cross-sectional area of the jet exit, sq in.

MODEL AND INSTRUMENTATION

Figure 1 is a three-view drawing of the model. In figures 2 and 3, respectively, are shown dimensional cross-sectional area distribution of the components of the model and the nondimensional area distribution of the complete model. Fineness ratio of the equivalent body was 12.8. Figures 4 and 5 are photographs of the model, and a photograph of the model and booster rocket in launching position is presented as figure 6. Physical dimensions of the model are included in table I.

The model was constructed primarily of aluminum and mahogany, with the exception of the jet-simulating solid-fuel rocket-motor case, which was of steel. The simulator motor was a modified Cordite rocket, and developed about 500 pounds of thrust for 4 seconds. The wing was of solid aluminum.

Contained within the model was a six-channel telemeter transmitter. Each channel monitored one of the following quantities: angle of attack, longitudinal acceleration, normal acceleration, free-stream total pressure, simulator motor chamber pressure, and jet-exit static pressure. Also contained within the model were six pulse rockets, timed by means of delay squibs to disturb the model in pitch at preset times during the flight.

The nozzle of the jet simulator motor, which had a sonic exit, was canted downward 5° with respect to the model reference line, in order to prevent pitching moments about the center of gravity as a result of thrust. The simulator-motor chamber-pressure orifice was located just inside the motor nozzle; the static-pressure orifice was located on the base of the model.

Ground instrumentation included two telemeter receiving stations, several tracking cameras, a CW Doppler radar set, an SCR-584 radar set, and rawinsonde atmospheric recording equipment.

TEST TECHNIQUE

Prior to the flight test, the jet simulator was ground tested. Quantities measured were thrust, chamber pressure, and free-stream static pressure. These measurements were used, in conjunction with chamber pressure and free-stream static pressure measured in flight, to determine simulator thrust during flight.

The model was boosted to $M = 1.58$ by a solid-fuel Deacon rocket motor developing about 6,000 pounds of thrust for 3 seconds. The model then separated from the booster rocket and coasted free, decelerating to $M = 1.075$. At $M = 1.075$, the simulator rocket motor started, and in the ensuing 4 seconds the model accelerated to $M = 1.34$. At $M = 1.34$, the simulator rocket fuel having been consumed, the model once again coasted free, decelerating to subsonic speeds.

Throughout the flight, data were transmitted continuously by the telemeter located in the model, and recorded on film at the two ground-receiving stations. The model was tracked in flight by the two radar sets, one of which was used to obtain model velocity, the other recording position in space. All telemeter and radar data were synchronized by a master timer; thereby, a time history of the quantities measured was provided.

Immediately after the flight, a balloon carrying rawinsonde weather equipment was released. Wind direction and velocity and atmospheric pressure, temperature, and density were thereby measured for the entire altitude range traversed by the model flight test.

METHOD OF ANALYSIS

Prior to analysis, the data were reduced by the Langley Instrument Research Division. Indicated angle of attack was corrected for flight-path curvature, and normal and longitudinal accelerations were corrected for pitch rate. Corrections have also been applied for fuselage bending due to heating from the simulator motor. No corrections have been made for aeroelasticity. Values of Mach number obtained from radar data and from telemeter data were plotted together, and a mean curve drawn through the points. The curve thus obtained was taken as the Mach number for this investigation.

Lift coefficient was

$$C_L = C_N = \left(\frac{a_n}{g}\right)\left(\frac{W}{qS}\right)$$

where a_n/g was the normal accelerometer reading, and C_L was assumed equal to C_N since the model flew near zero lift.

External-drag coefficient was calculated by two methods for both the power-on and the power-off phases of the flight.

$$C_D = C_T - \left(\frac{dV}{dt} - 32.2 \sin \gamma\right)\left(\frac{W}{qS}\right) \tag{1}$$

where dV/dt was obtained by differentiation with respect to time of the velocity as obtained from CW Doppler radar. Thrust coefficient C_T was obtained from telemeter data in conjunction with the preflight test of the simulator rocket motor, as discussed previously. For the power-off case, C_T was defined as

$$C_T = \left(\frac{p_j - p_\infty}{q}\right)\left(\frac{A_{nozzle}}{S}\right)$$

Hence, the power-off drag coefficient has been corrected to zero pressure drag on the base of the nozzle exit. Base drag on the small annular area surrounding the nozzle exit is considered part of the external drag.

$$C_D = C_C = C_T - \left(\frac{a_l}{g}\right)\left(\frac{W}{qS}\right) \tag{2}$$

where a_l/g was obtained from telemeter data and C_D was assumed equal to C_C since the model flew near zero lift. C_T was calculated by the method described in equation (1). Values of drag coefficient from equations (1) and (2) were plotted and a mean curve drawn through the points. The curve thus obtained was taken as the external-drag coefficient, both power-on and power-off, for the test reported herein.

A more complete description of the test technique and method of analysis may be found in reference 6.

As may be seen in figure 1, the nozzle of the jet was canted downward 5° with respect to the fuselage reference lines, which allowed the thrust axis to pass very nearly through the center of gravity of the model. Effects of propellant consumption on the center-of-gravity location were investigated and found to have negligible effect on trim.

ACCURACY

Mach number measurements are believed to be accurate within ±0.01, drag coefficient within ±0.001 power off and ±0.003 power on, lift coefficient within ±0.003, and angle of attack within ±0.1°. The figures quoted are maximum probable values, and in general the errors are appreciably smaller than the quoted numbers.

DISCUSSION OF RESULTS

Reynolds number for the test reported herein, based on mean aerodynamic chord, varied from about 3.2×10^6 to about 13.0×10^6 at Mach numbers from 0.88 to 1.58, respectively, as shown in figure 7. The center of gravity was located 25 percent behind the leading edge of the mean aerodynamic chord and about 17 percent below the wing chord plane for both the power-on and the power-off condition. Jet-off data were obtained at Mach numbers from 0.88 to 1.56, whereas jet-on data were limited to a Mach number range of 1.09 to 1.34.

Jet static-pressure ratio increased from 2.8 at $M = 1.09$ to 3.3 at $M = 1.34$, as may be seen in figure 8. Thrust coefficient decreased from 0.102 at $M = 1.09$ to 0.085 at $M = 1.34$, as shown in figure 9. These values correspond approximately to a turbojet powered airplane with a sonic exit capable of supersonic speed.

Longitudinal Trim

Trim lift coefficient is presented as a function of Mach number in figure 10(a). It will be noted that there were no abrupt trim changes, either jet-on or jet-off, with respect to changes in Mach number. In figure 10(b), effect of the jet on the trim lift coefficient is shown to decrease in magnitude from about -0.034 at $M = 1.09$ to a value of -0.021 at $M = 1.34$. Reference 5 shows a similar effect of the jet on trim for a model of similar (overhanging tail boom) configuration. In reference 5, however, jet pressure ratio and thrust coefficient were greater than for the present test, hence the change in trim was greater. It is interesting to note, however, that the trends were similar, that is, a decrease in jet effect on trim at Mach numbers above 1.2. This effect agrees with trends shown in reference 1 which indicate that, for a horizontal surface located above and behind the jet-exit shock, the increment in normal-force coefficient decreases in magnitude with increasing Mach number. It should be noted that the jet-on trim lift coefficient shown in figure 10(a) includes an increment due directly to the 5° cant angle of the jet nozzle. Since the nozzle cant angle is considered an integral part of the configuration reported herein, this increment has not been taken out as a tare. Its magnitude is approximately $\Delta C_{L_{trim}} = 0.008$.

Figure 11(a) shows trim angle of attack for both the jet-on and the jet-off condition. For the jet-off condition, the variation in trim angle of attack was about 0.8° over the Mach number range. As may be seen in figure 11(b), effect of the jet on the trim angle of attack was only slightly affected by Mach number; the increment was about -0.8° over the Mach number range.

Drag

External-drag coefficient is shown as a function of Mach number in figure 12 for both the jet-on and the jet-off conditions. In figure 12(a), C_D for the jet-off condition is shown to rise from a subsonic value of about 0.018 to a supersonic level of about 0.0255. The drag rise $\left(\text{where } \frac{dC_D}{dM} = 0.1\right)$ occurred at $M = 0.98$. Model 2 of reference 7, shown for comparison, also had its drag rise at $M = 0.98$. The model of reference 2, which was similar to the model of this test, but had an open

inlet, had appreciably less jet-off drag at subsonic speeds than the model of this test, but at transonic and supersonic speeds the jet-off drag levels of the models are about the same. The increment between the models at subsonic speeds is believed to be due in part to the smaller wetted area and smoother finish of the reference model. The higher pressure drag (of the reference model) is believed to be the result of its lower fineness ratio. Jet-on drag coefficient for the model of this test increased steadily from a value of about 0.019 at $M = 1.09$ to about 0.029 at $M = 1.34$.

Figure 12(b) shows jet effect on drag coefficient to decrease steadily in magnitude from -0.006 at $M = 1.09$ to zero at $M = 1.27$, then to increase to 0.003 at $M = 1.34$. Data from reference 8, also shown in figure 12(b), show the same trend for a horizontal-tailless, delta-wing model with an overhanging tail boom. Other tests (unpublished) have shown the same trend. In general, it appears that for a configuration with an overhanging tail boom, similar to the model of this test, the jet can be expected to decrease the drag at Mach numbers near 1.1, and to increase the drag at Mach numbers above about 1.2. The favorable effect of the jet on the drag at near-sonic speeds is probably due in part to the jet stream improving the overall area distribution of the airplane.

Shown in figure 3 is an approximation of the jet-area distribution and how it may improve the total-area distribution in the region of the steep slopes near $x/l = 0.7$. Such an improvement, according to the transonic area rule, would indicate a reduction in the transonic drag rise.

Lift

Lift-curve slope is shown in figure 13. Jet effect on lift-curve slope was very slight. Also shown in figure 13 for comparison is the lift-curve slope of a configuration having a similar wing plan form from reference 9, and an identical plan form from unpublished data. Agreement between the reference data and the power-off data of this test is good.

Figure 14(a) presents angle of attack corresponding to zero lift for both the jet-on and jet-off conditions. Effect of the jet on the angle of attack for zero lift is shown in figure 14(b). The increment is negative over the entire range tested, but does not exceed -0.4° at any Mach number.

In figure 15, lift coefficient corresponding to zero angle of attack is shown as a function of Mach number for the jet-on and jet-off conditions.

For the jet-on condition, the values of lift coefficient are small and positive throughout the Mach number range tested; for the jet-off condition, the values are small and generally negative. Effect of the jet on the lift coefficient at zero angle of attack is shown directly in figure 16. The increment is positive (about 0.02) over the tested Mach number range.

SUMMARY OF RESULTS

A rocket-powered free-flight model of an interceptor-type airplane with an overhanging tail boom was flight tested with jet on and jet off at Mach numbers from 1.09 to 1.34. Reynolds numbers varied from 5.0×10^6 to 10.2×10^6, respectively. Jet static-pressure ratio increased from 2.85 at a Mach number of 1.09 to 3.3 at a Mach number of 1.34. The following conclusions are indicated by this test:

1. Effect of the jet on the low-lift drag coefficient decreased steadily from -0.006 at a Mach number of 1.09 to zero at a Mach number of 1.27, then increased to 0.003 at a Mach number of 1.34.

2. Jet effect on the trim lift coefficient decreased in magnitude from -0.034 at a Mach number of 1.09 to -0.021 at a Mach number of 1.34.

3. Effect of the jet on the airplane lift-curve slope was slight.

4. Lift coefficient corresponding to zero angle of attack was increased moderately by the jet.

Langley Aeronautical Laboratory,
National Advisory Committee for Aeronautics,
Langley Field, Va., June 19, 1957.

REFERENCES

1. Bressette, Walter E., and Faget, Maxime A.: An Investigation of Jet Effects on Adjacent Surfaces. NACA RM L55E06, 1955.

2. Cornette, Elden S., and Ward, Donald H.: Transonic Wind-Tunnel Investigation of the Effects of a Heated Propulsive Jet on the Pressure Distribution Along a Fuselage Overhang. NACA RM L56A27, 1956.

3. Henry, Beverly Z., Jr., and Cahn, Maurice S.: Preliminary Results of an Investigation at Transonic Speeds To Determine the Effects of a Heated Propulsive Jet on the Drag Characteristics of a Related Series of Afterbodies. NACA RM L55A24a, 1955.

4. Englert, Gerald W., Wasserbauer, Joseph F., and Whalen, Paul: Interaction of a Jet and Flat Plate Located in an Airstream. NACA RM E55G19, 1955.

5. Peck, Robert F.: Jet Effects on Longitudinal Trim of an Airplane Configuration Measured at Mach Numbers Between 1.2 and 1.8. NACA RM L54J29a, 1955.

6. Gillis, Clarence L., Peck, Robert F., and Vitale, A. James: Preliminary Results From a Free-Flight Investigation at Transonic and Supersonic Speeds of the Longitudinal Stability and Control Characteristics of an Airplane Configuration With a Thin Straight Wing of Aspect Ratio 3. NACA RM L9K25a, 1950.

7. Judd, Joseph H.: A Free-Flight Investigation of the Drag Coefficients of Two Single-Engine Supersonic Interceptor Configurations From Mach Number 0.8 to 1.90 To Determine the Effect of Inlet and Engine Locations. NACA RM L55G05a, 1955.

8. Judd, Joseph H., and Falanga, Ralph A.: Flight Investigation of the Effect of a Propulsive Jet Positioned According to the Transonic Area Rule on the Drag Coefficients of a Single-Engine Delta-Wing Configuration at Mach Numbers From 0.83 to 1.36. NACA RM L56A16, 1956.

9. Blanchard, Willard S., Jr.: A Summary of the Low-Lift Drag and Longitudinal Trim Characteristics of Two Versions of an Interceptor-Type Airplane As Determined From Flight Tests of Rocket-Powered Models at Mach Numbers Between 0.75 and 1.78. NACA RM L54H31, 1954.

TABLE I.- GEOMETRIC DIMENSIONS

Wing:	
Total area, sq ft	3.84
Aspect ratio	3.40
Sweepback (quarter chord), deg	52.5
Taper ratio	0.20
Mean aerodynamic chord, ft	1.37
Section (parallel to free stream)	NACA 65A004
Horizontal tail:	
Total area, sq ft	0.61
Aspect ratio	3.40
Sweepback (quarter chord), deg	52.5
Taper ratio	0.20
Section (parallel to free stream)	NACA 65A004
Vertical tail:	
Total area (to center line), sq ft	0.94
Aspect ratio (to center line)	1.70
Sweepback (quarter chord), deg	52.5
Taper ratio	0.20
Section (parallel to center line)	NACA 65A004
Fuselage:	
Frontal area, sq ft	0.27
Length, ft	7.64
Base area, sq ft	0.08
Location of leading edge of horizontal-tail mean aerodynamic chord downstream from jet exit, ft	0.76
Location of horizontal-tail chord plane above jet exit, ft	0.34
Diameter of jet exit, ft	0.32

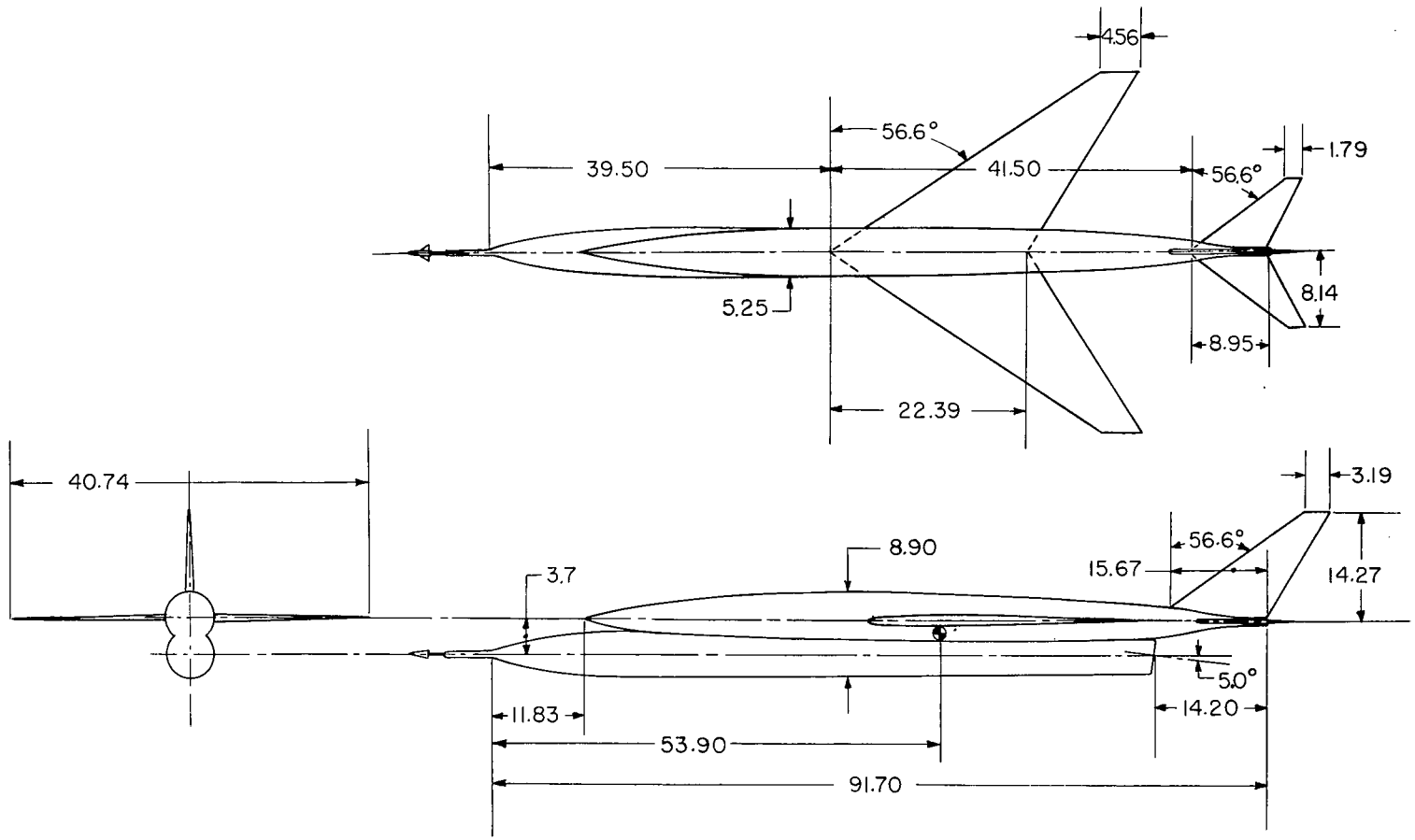

Figure 1.- Three-view drawing of the model tested. All dimensions are in inches unless otherwise noted.

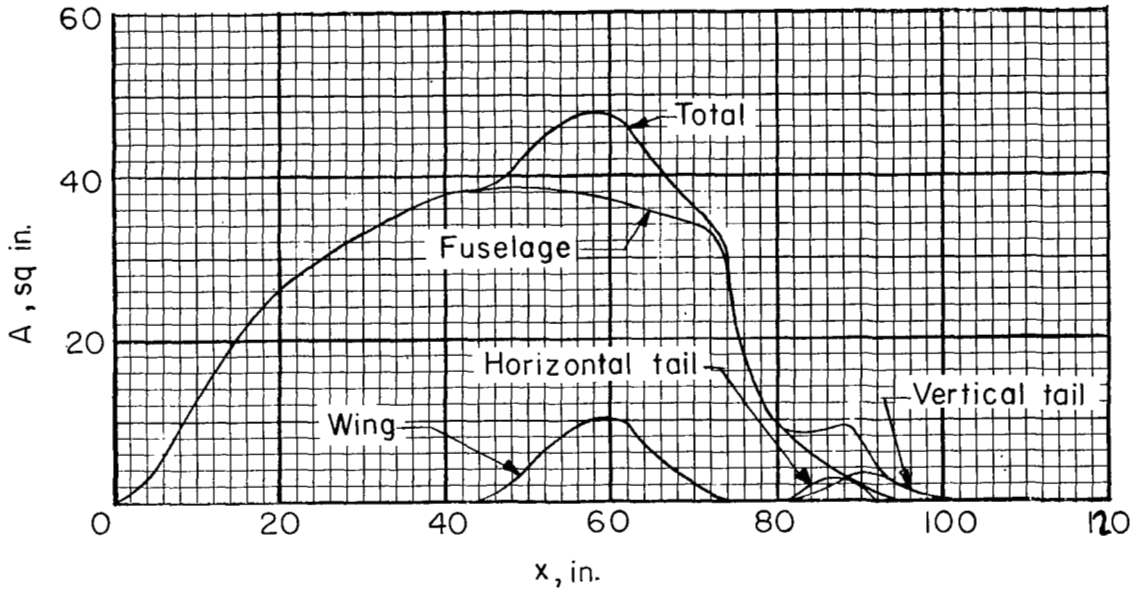

Figure 2.- Dimensional cross-sectional area of the components.

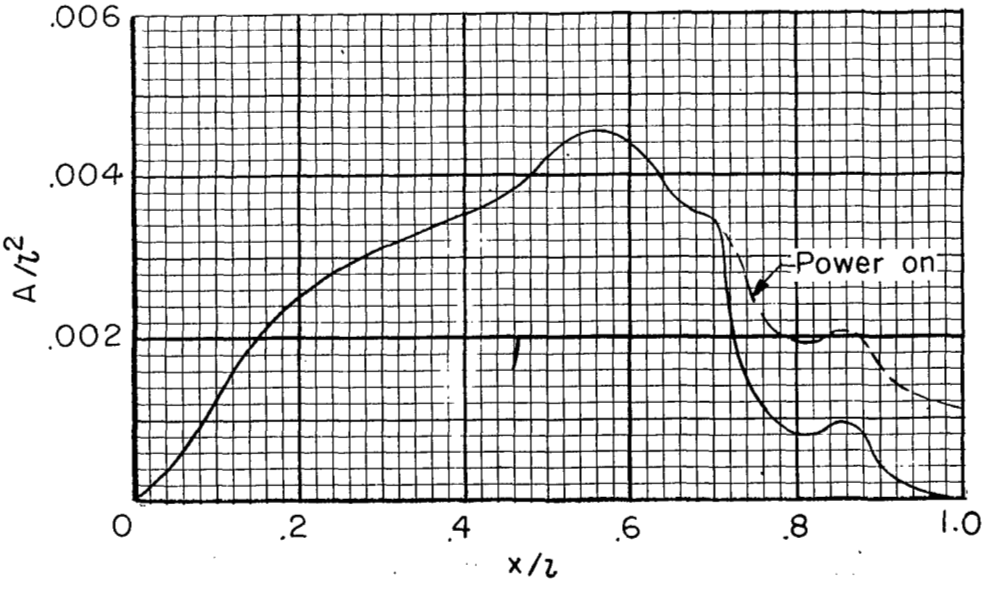

Figure 3.- Nondimensional cross-section of the complete model.

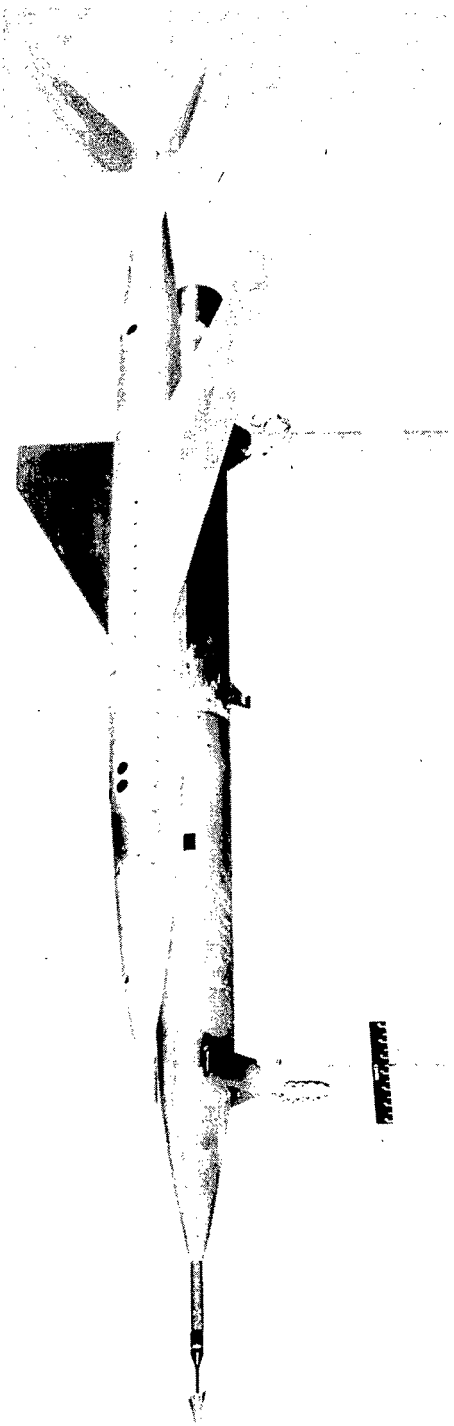

Figure 4.- Quarter-front view of the test model. L-88849.1

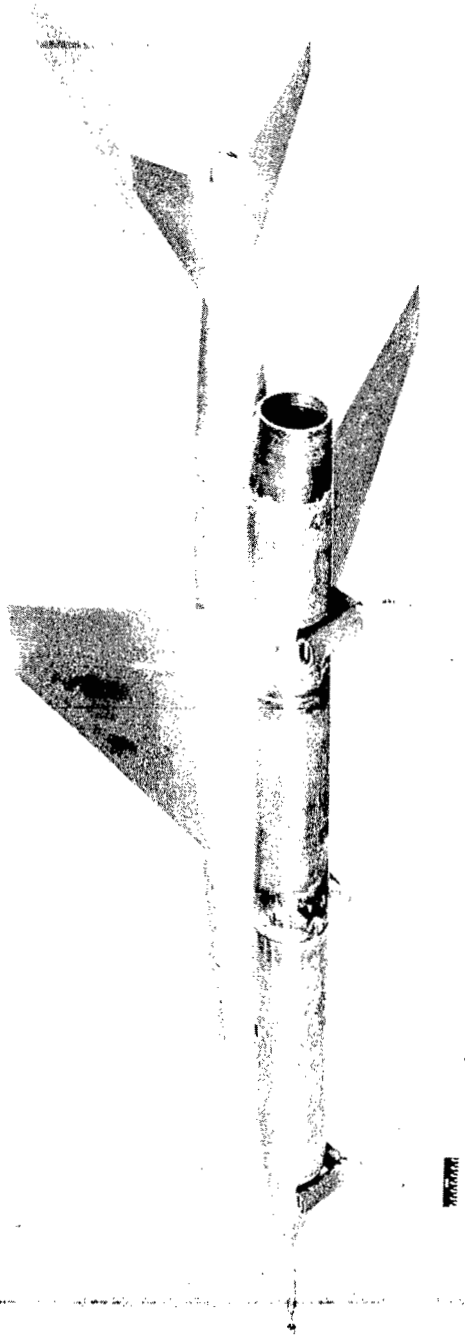

Figure 5.- Quarter-rear view of the test model. L-88850.1

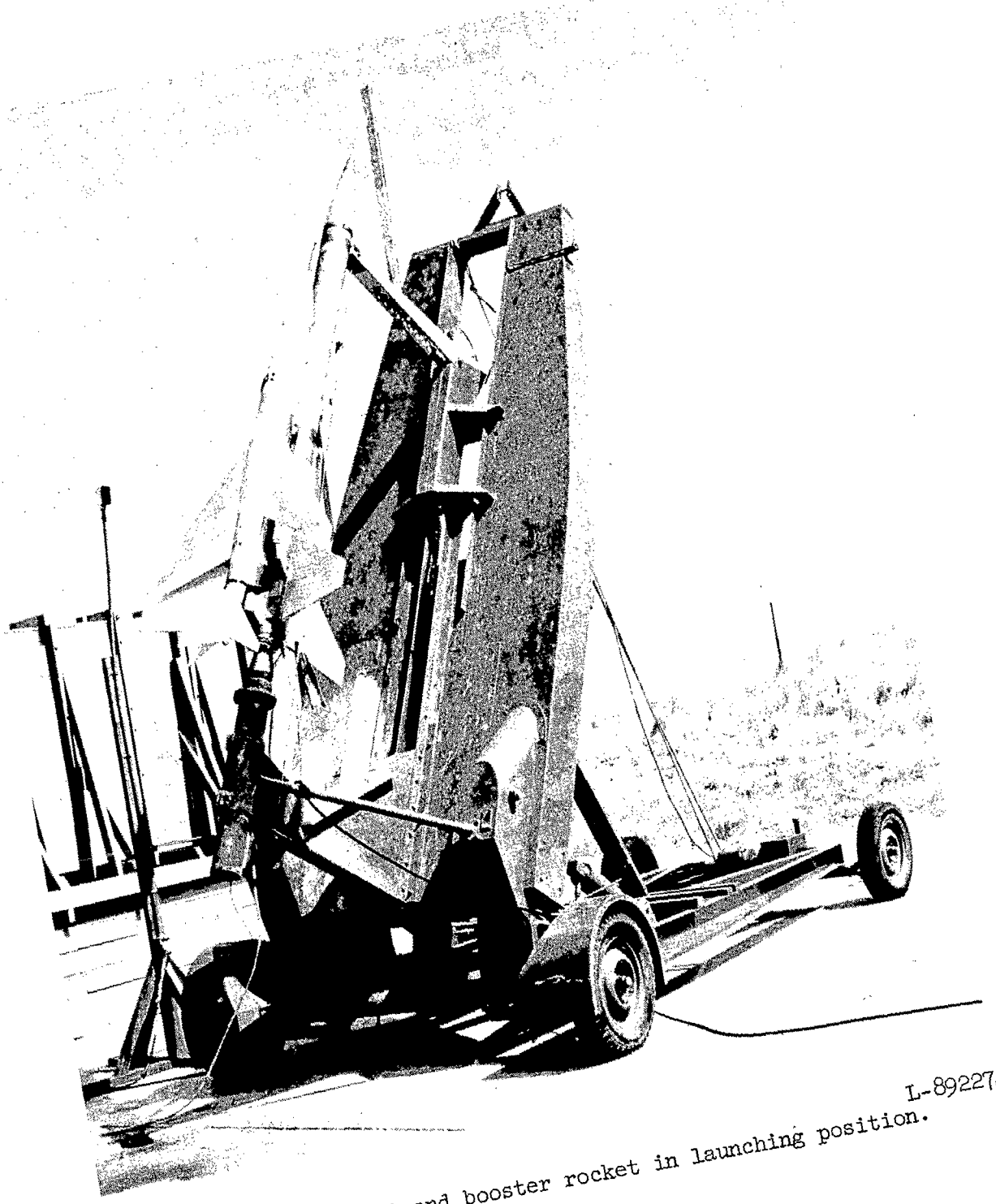

L-89227.1

Figure 6.- Model and booster rocket in launching position.

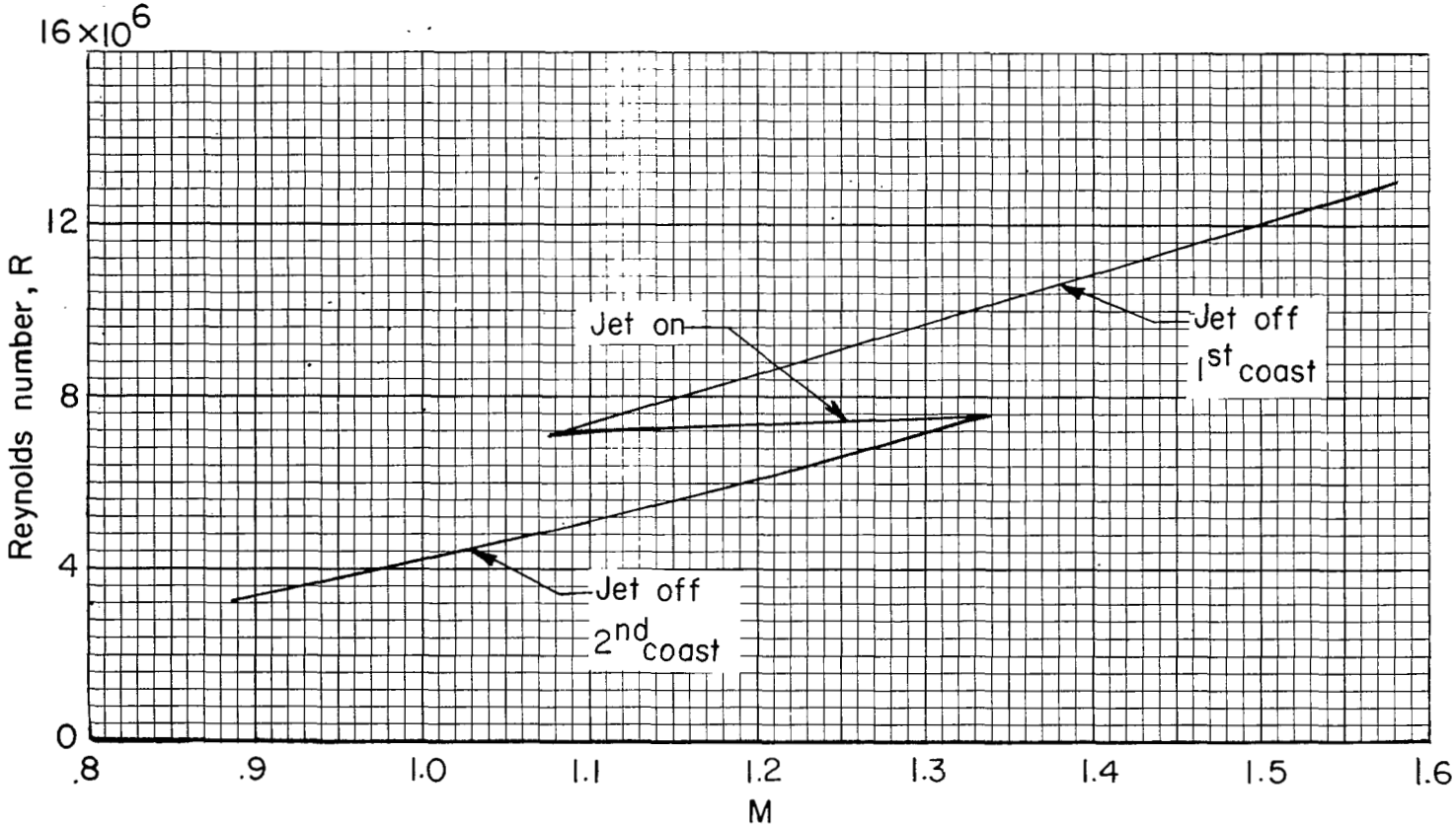

Figure 7.- Variation of Reynolds number with Mach number.

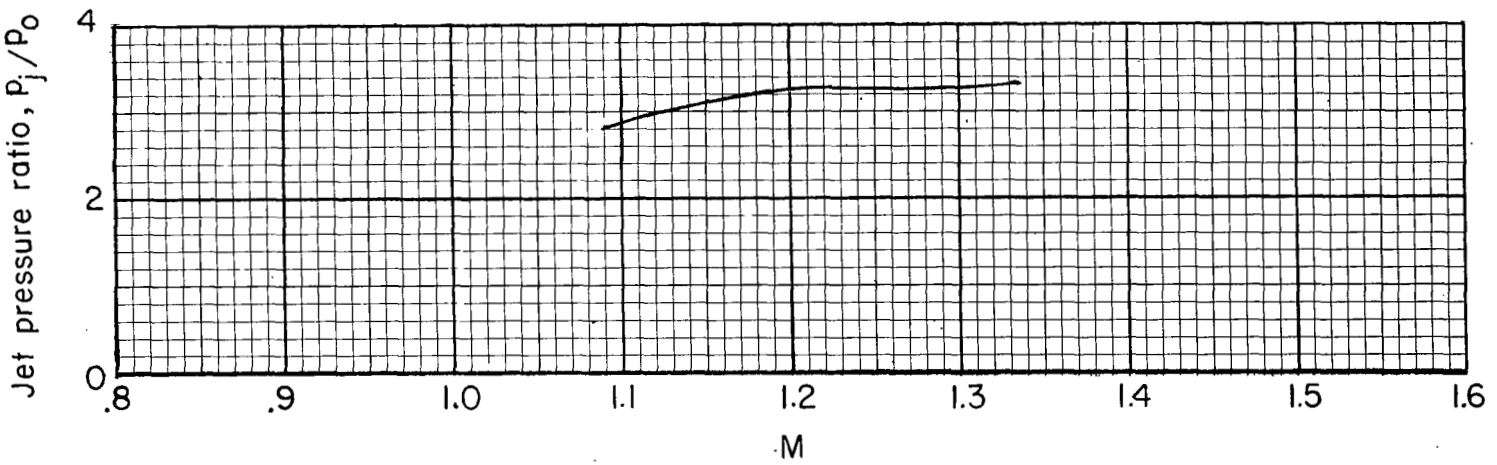

Figure 8.- Jet static-pressure ratio during the power-on portion of the flight test.

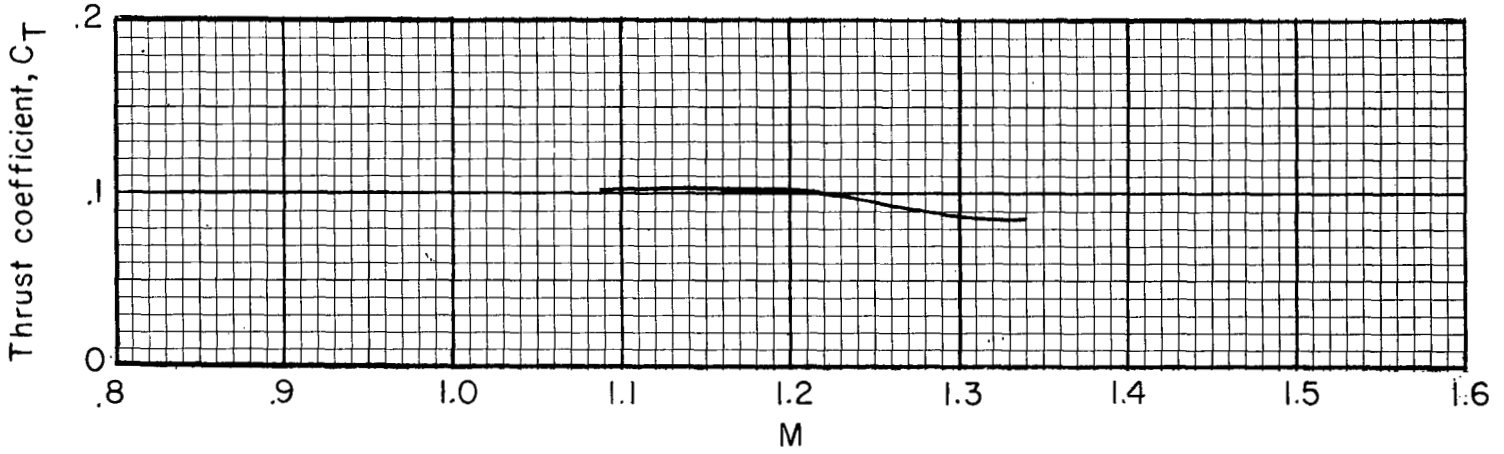

Figure 9.- Thrust coefficient.

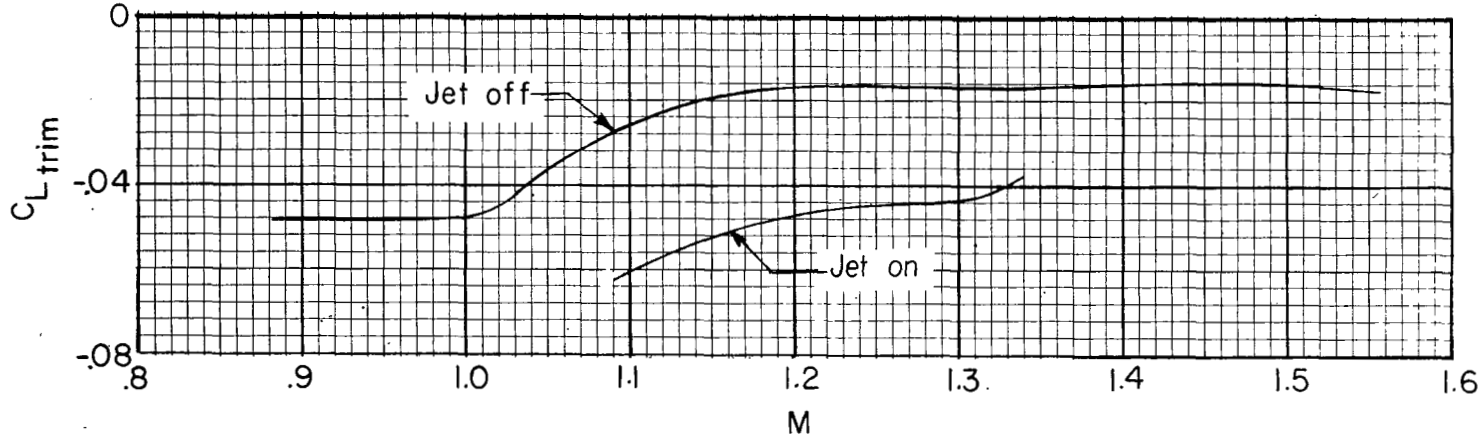

(a) Jet on and jet off.

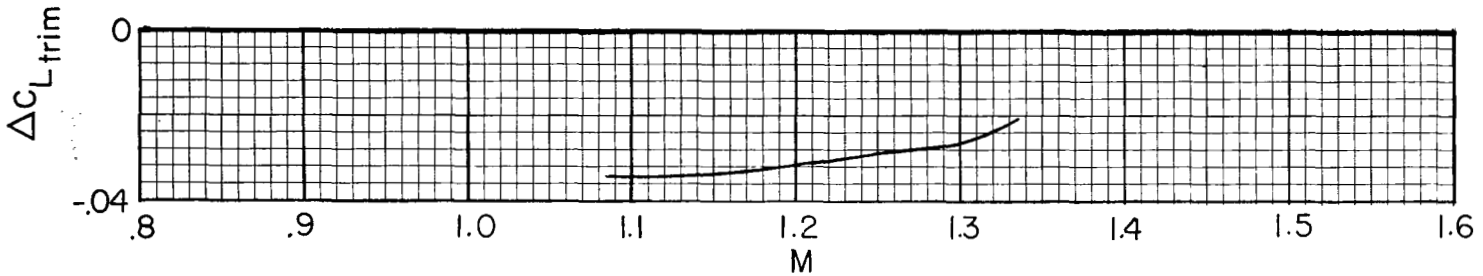

(b) Effect of jet on the longitudinal trim.

Figure 10.- Trim lift coefficient.

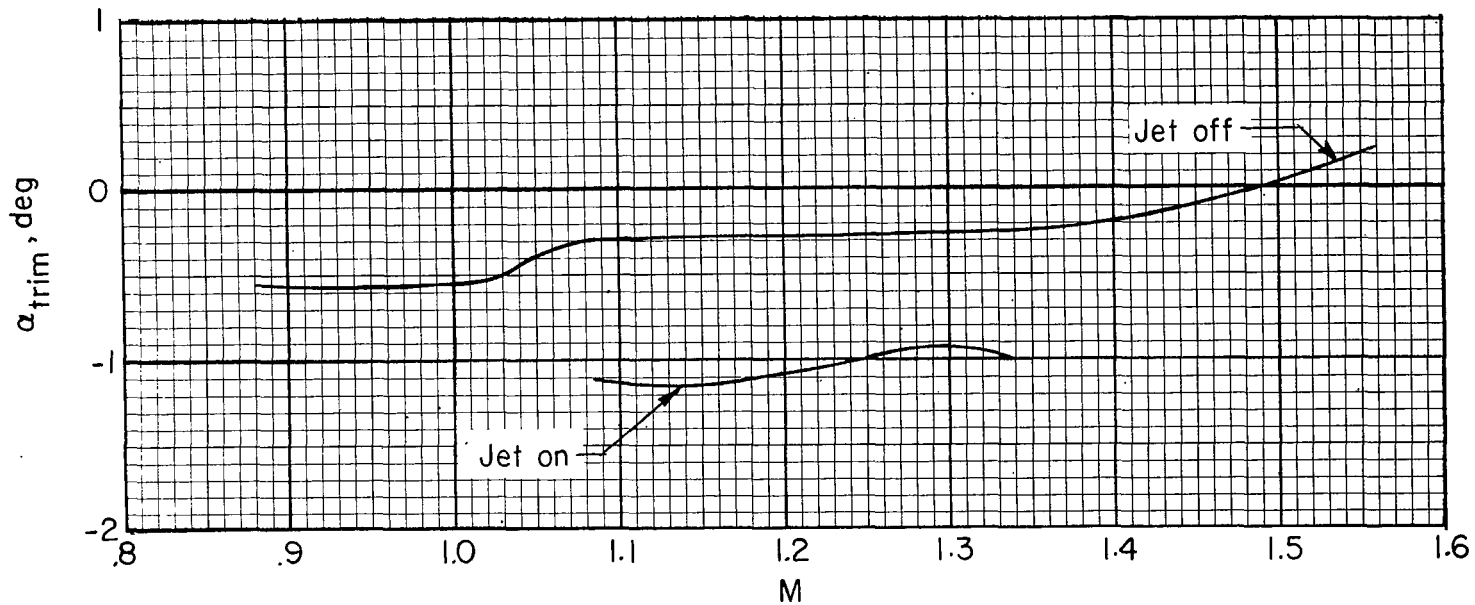

(a) Jet on and jet off.

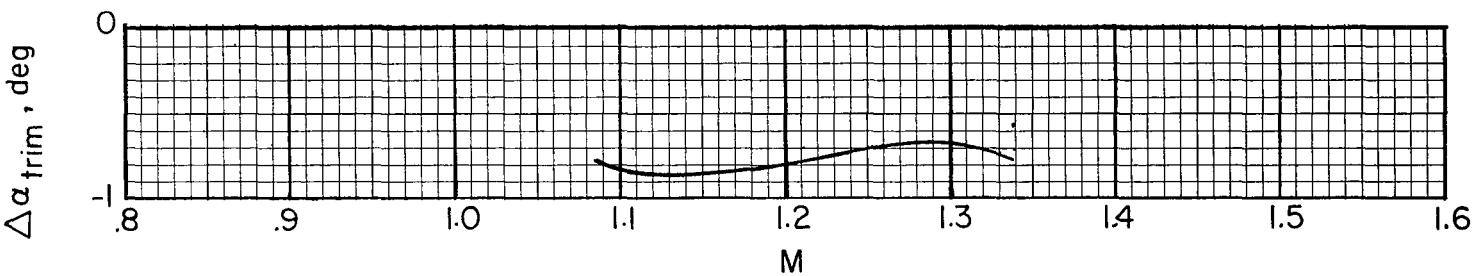

(b) Effect of jet on the longitudinal trim.

Figure 11.- Trim angle of attack.

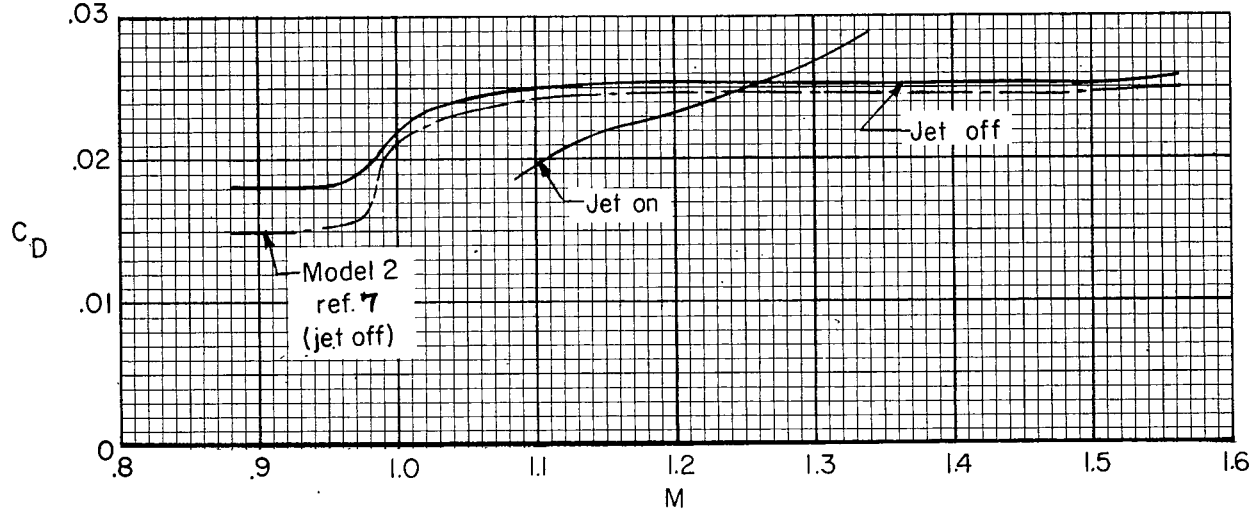

(a) Jet on and jet off.

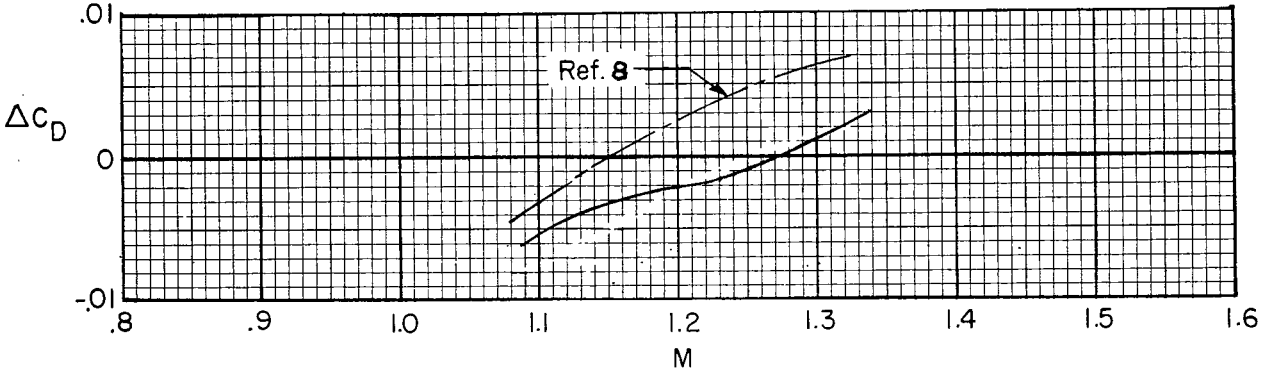

(b) Effect of jet on the drag.

Figure 12.- Low-lift drag coefficient.

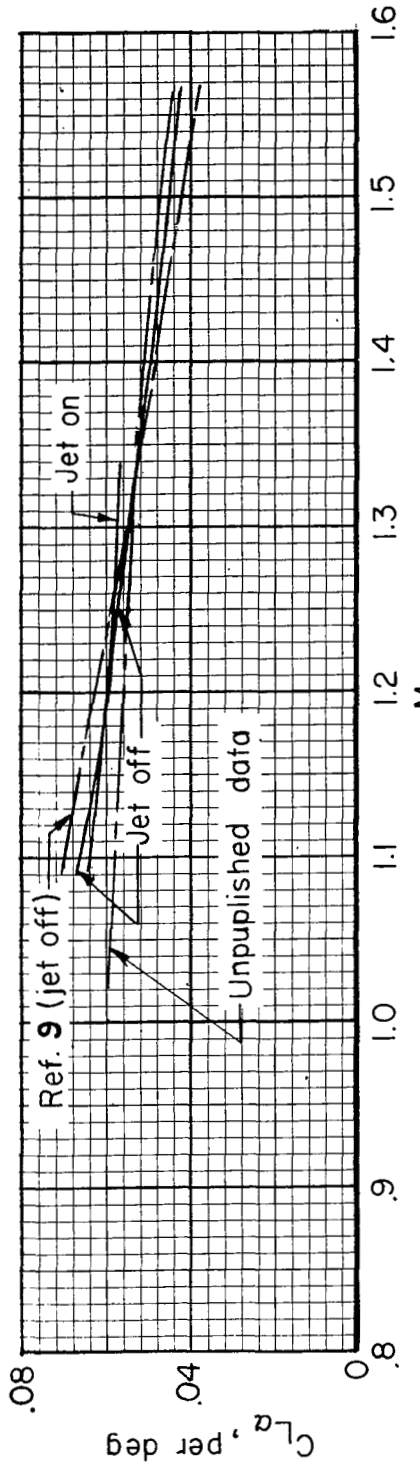

Figure 13.- Lift-curve slope.

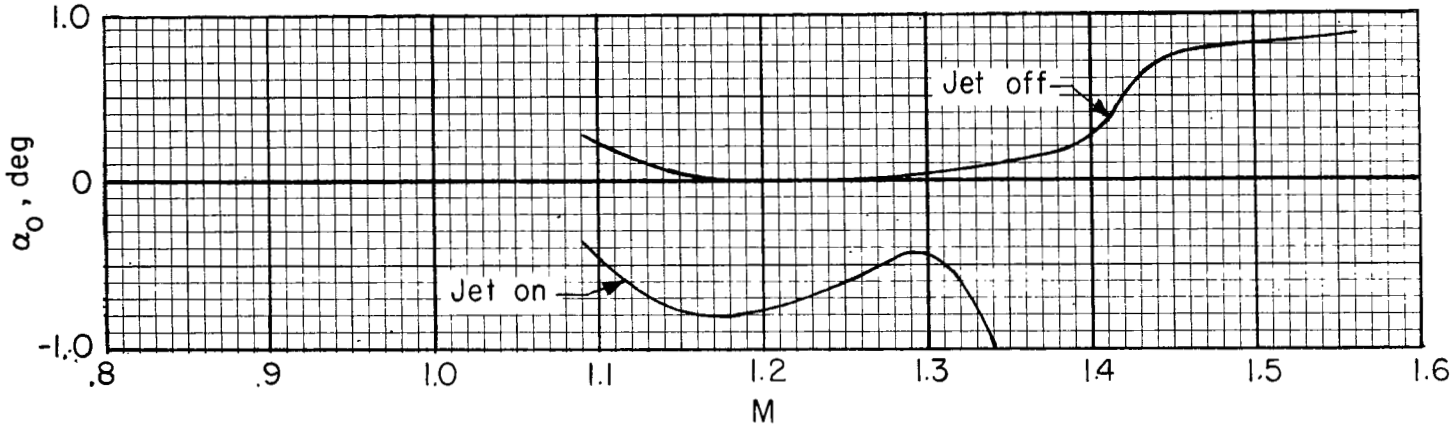

(a) Jet on and jet off.

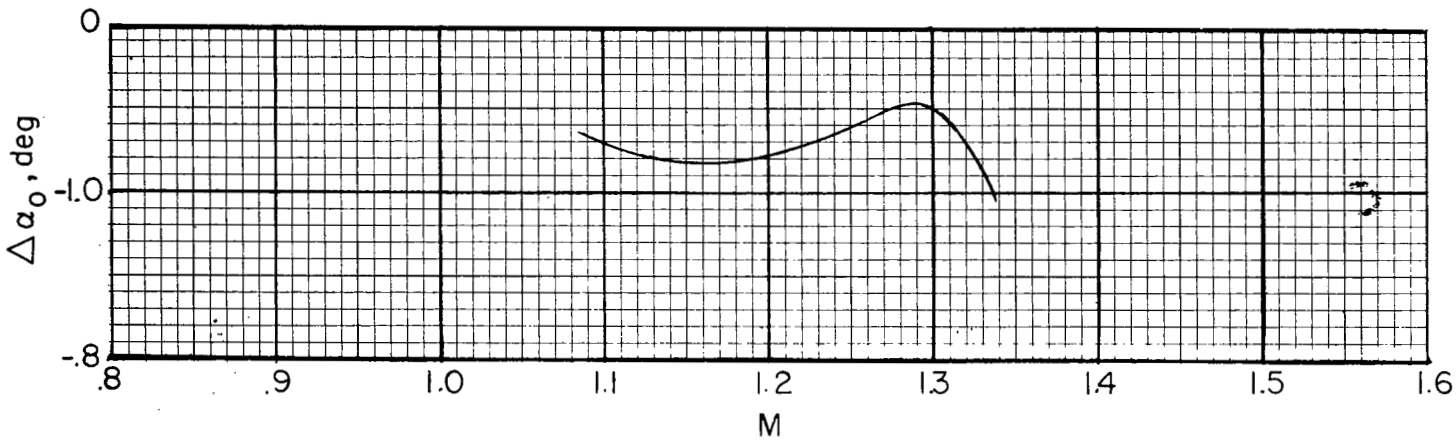

(b) Jet effect.

Figure 14.- Angle of attack corresponding to zero lift.

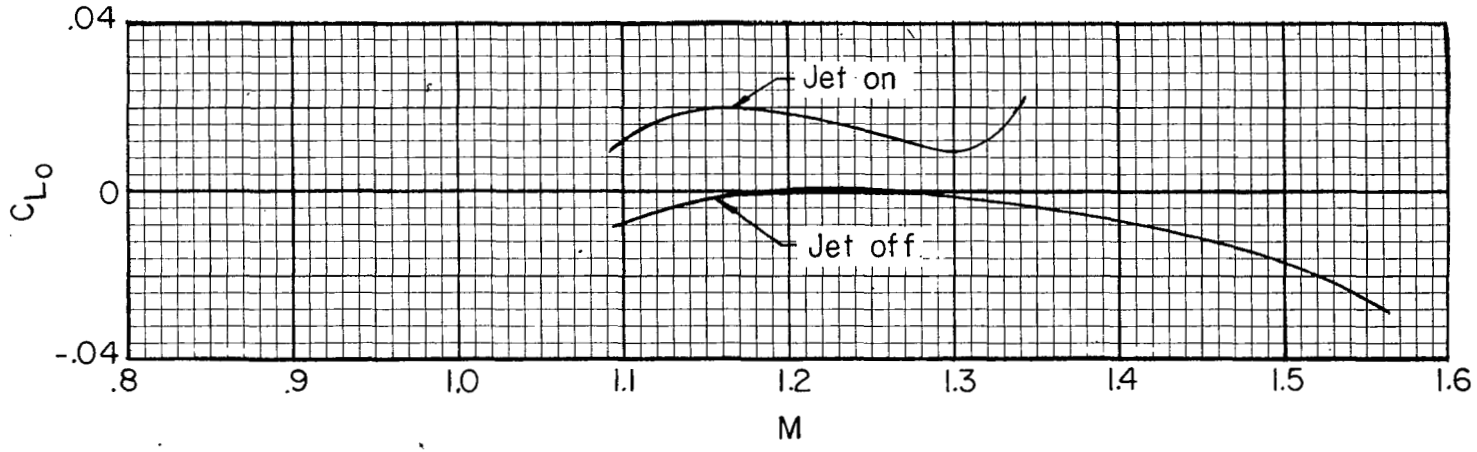

Figure 15.- Lift coefficient at zero angle of attack.

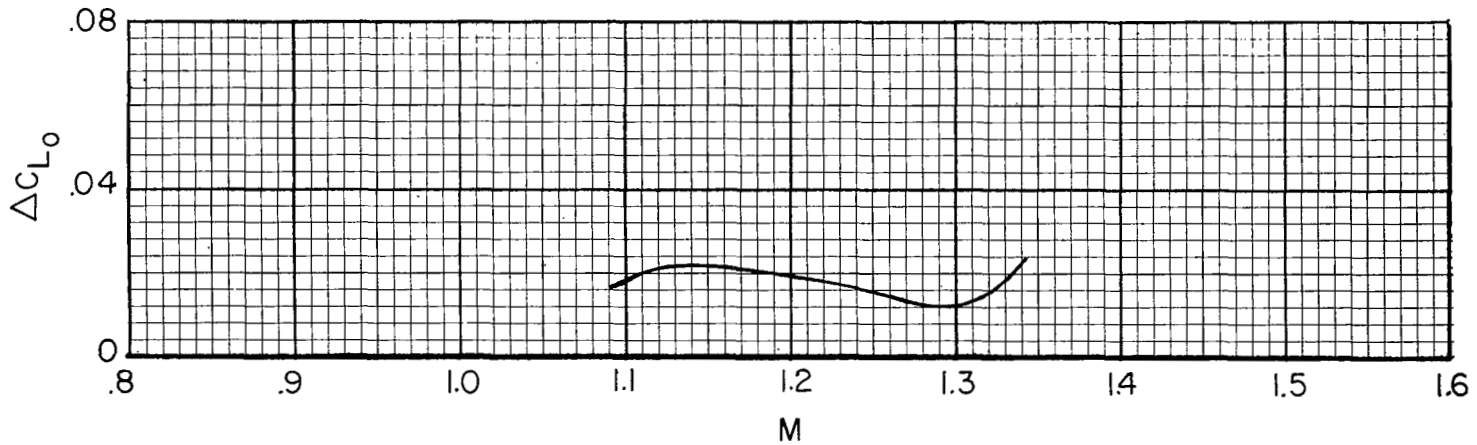

Figure 16.- Effect of jet on the lift coefficient at zero angle of attack.